Cellulose Nanofibrils from Corncobs and Their Nanocomposite with Alginate: Study of Swelling Behavior

Agus Wedi Pratama [1,2] [ID] , **Hardian Susilo Addy** [3] [ID] , **Nurul Widiastuti** [2] [ID] , **Alvin Rahmad Widyanto** [2] [ID] , **Anisa Ratnasari** [4] [ID] , **Dwi Indarti** [5] [ID] , **Bambang Piluharto** [5,*] [ID]

[1] Graduate School of Biotechnology, University of Jember, Kampus Tegal Boto, Jember 68121, East Java, Indonesia; aguswedi445@gmail.com (A.W.P.);

[2] Department of Chemistry, Faculty of Science and Data Analytics, Institut Teknologi Sepuluh Nopember, Surabaya 60111, East Java, Indonesia; nurul.widiastuti@chem.its.ac.id (N.W.);

[3] Department of Plant Protection, Faculty of Agriculture, University of Jember, Kampus Tegal Boto, Jember 68121, East Java, Indonesia; hsaddy.faperta@unej.ac.id (H.S.A.);

[4] Department of Environmental Engineering, Faculty of Civil, Planning and Geo-Engineering, Institut Teknologi Sepuluh Nopember, Surabaya 60111, East Java, Indonesia

[5] Department of Chemistry, Faculty of Mathematics and Natural Sciences, University of Jember, Kampus Tegal Boto, Jember 68121, East Java, Indonesia; bampito.fmipa@unej.ac.id (B.P.);

* Correspondence: bampito.fmipa@unej.ac.id (B.P.);

Abstract: In this study, isolated cellulose from corncobs was oxidized using 2,2,6-tetramethyl-1-piperidinyl oxy (TEMPO) to produce cellulose nanofibrils. Cellulose nanofibrils were characterized by FTIR, PSA, and zeta potential to determine their chemical structure, particle size, and surface charge. Subsequently, the obtained cellulose nanofibrils were incorporated into the alginate matrix to produce composite beads. The effects of cellulose nanofibrils and alginate composition in composite beads were studied on the physical properties such as diameter size, morphology, drying rate, and swelling behavior. The result figures out a new chemical structure in the cellulose nanofibrils spectrum after the treatment process. The content of surface charges increases three times after the treatment process, from 0.2 to 0.64 mmol/g. The average size of cellulose nanofibril suspension particles was 153,4, with a polydispersity index of 0.044 (the nanofiber range). The zeta potential value is -46.3 mV, demonstrating the good stability and dispersibility of the cellulose nanofibril particles. The diameter of composite Alginate-Cellulose Nanofibril (AC) beads was reduced from 4.003 to 3.078 mm in AC20 by increasing the cellulose nanofibril concentration. The capacity of alginate beads to absorb water was 30% higher than that of the composite AC beads. Based on SEM analysis, the morphology of AC beads was found to be finer and denser than that of alginate beads. The swelling kinetics of the beads indicate that the diffusion mechanism is a Fickian diffusion mechanism. Furthermore, cellulose nanofibril-added beads can potentially be used as smart materials in bioactive encapsulated applications owing to having good swelling properties.

Keywords: nanocellulose; alginate beads; corncobs; swelling study; nanocomposite.

1. Introduction

Alginate is a natural water-soluble polymer with good biodegradability and biocompatibility properties [1]. Alginate is produced from brown seaweeds and is frequently utilized as an encapsulating agent to preserve bioactive substances from environmental conditions [2]. Calcium ion crosslinking was employed extensively in the production of alginate

beads. Alginate beads have been developed for the encapsulation of bioactive substances, including *Saccharomyces cerevisiae* [3], protein, biochar [4], and black seed oil [5].

Over the past decade, the formation of alginate beads without reinforcement materials still has several limitations, including low mechanical strength, high porosity, low stability, and high swelling of the bead network in the presence of monovalent ions so that the bioactive encapsulated is easily released [6]. To overcome the limitation, reinforced material can be used to compensate for the unfavorable properties of the alginate beads matrix. In addition, the addition of reinforcement material is able to improve swelling performance. Previous studies utilized bentonite as a reinforcing material to encapsulate *Beauveria bassiana* [7], *Lactobacillus rhamnosus* GG [8], and amoxicillin [9]. Even though bentonite has better performance in decreasing the swelling degree of beads, bentonite is an inorganic material that has no compatibility with bioactive. Thus, using organic materials, such as biopolymers, is more promising than using inorganic materials in terms of compatibility with bioactive. Furthermore, biopolymer is abundant, biodegradable, and renewable. Cellulose is one of the biopolymers composed of glucose monomers and is widely used in various fields as a source for advanced materials, such as composites made from cellulose fibers [10]. Plant cell walls can be isolated as a cellulose source to obtain cellulose fibers. Thus, cellulose fibers can be modified in nano size and their chemical structure to obtain superior properties that are called cellulose nanofibrils and cellulose nanocrystal. However, cellulose nanocrystals have significant limitations, including low thermal stability, high water usage, and environmental incompatibility caused by the use of sulfuric acid. In addition, Cellulose nanocrystals are typically more expensive and have lower mechanical strength than cellulose nanofibrils. Thus, cellulose nanofibrils are more suitable for alginate beads' reinforcement material [11]. Cellulose nanofibrils have strong bonding with alginate because of the presence of hydrogen bonding and surface charge.

Several methods have been proposed to synthesize cellulose nanofibrils, including two-step oxidations of periodate and sodium chlorite, nitric acid oxidation, and TEMPO oxidation [12]. Compared to TEMPO oxidation, two-step oxidations of periodate and sodium chlorite are not as simple due to the need for two steps to finish the formation of cellulose nanofibrils. In addition, it indicates an unaffordable technique. As well as two-step oxidations of periodate and sodium chlorite, nitric acid oxidation is an uncompromising technique since it needs to form HNO_2 before forming cellulose nanofibrils. Hence, TEMPO oxidation is a viable approach to synthesizing cellulose nanofibrils. Furthermore, aside from being a simple and inexpensive process, TEMPO oxidation delivers a negative charge to sodium carboxylate groups on the surface of cellulose nanofibrils [13]. Consequently, it is feasible to disperse them, resulting in nanofibril cellulose completely.

In this work, cellulose-sized fibers were fibrillated by mechanical sonication treatment after corncob-derived cellulose was processed with TEMPO oxidation. The products are then mixed into the alginate matrix to generate composite beads, and their characteristics are evaluated, particularly the swelling kinetics behavior, since, to the author's knowledge, research on the parameters of this swelling behavior is currently confined to beads containing nanofiller-based natural material, such as corncobs. Cellulose nanofibrils can form strong intermolecular interactions with the hydroxyl groups (-OH) present in the chemical structure of alginate, enhancing the physical properties of the resulting composite beads. The presence of surface charges on cellulose nanofibrils would enhance the value of the manufactured beads.

2. Materials and Methods

2.1. Materials.

Corncobs were collected from agricultural waste in Jember, East Java, Indonesia. 2,2,6,6-tetramethyl-1-piperidinyloxy, TEMPO (MW = 156.25, 98%), sodium chlorite (MW = 90.44, technical grade 80%), and sodium alginate (Viscosity: 15–25 cP, 1% in H_2O) were supplied by Sigma-Aldrich. Sulfuric acid (95.0–97.0 wt.%), hydrogen chloride, sodium hydroxide, potassium hydroxide, sodium bromide, and sodium hypochlorite were obtained from Merck.

2.2. Preparation of cellulose nanofibril.

2.2.1. Isolation of cellulose from corncobs.

Cellulose was obtained by isolating cellulose from lignin and other components of the corncob. The procedure of cellulose isolation with a slight modification was applied according to Silverio et al. [14]. Corncobs were mashed and sieved through a 250-micron sieve to obtain corncob powder. The corncob powder was then added to a refluxed and stirred NaOH solution (2% (w/w), 80 °C, 4 h). After that, the precipitated corncob powder was washed using distilled water to remove alkaline residues. Then, it was dried in an air-circulating oven (30 °C, 24 h) and bleached using a sodium chlorite aqueous solution (1.7 % (w/w), 80 °C, 4 h) under mechanical stirring. After stirring, the sample was washed in distilled water and dried in an air-circulating oven (30 °C, 24 h).

2.2.2. Extraction of cellulose nanofibril.

Cellulose nanofibrils were prepared using TEMPO-mediated oxidation, according to previous reports by Masruchin et al. [15]. The samples were ground using an aluminum mortar and passed through a 250 microns sieve for extracting cellulose nanofibrils with the TEMPO/NaBr/NaClO oxidation system at room temperature (23 °C) at pH 10.5. Two grams of sample were dispersed in a solution consisting of an oxidizing reagent (0.025 g TEMPO and 0.25 g NaBr, diluted with 150 mL distilled water). Oxidation is initiated by adding 8 mL of NaClO solution dropwise (12.5% purity) into the mixed solution to maintain a pH of 10. In this reaction, the pH of the mixture decreases due to the formation of the carboxylate group. As a result, the pH of the mixture was kept at 10.5 by adding 0.5 M NaOH solution dropwise. The reaction was completed until there was no further change in the pH of the mixture. After the treatment, 0.5 M HCl solution was added to the mixture until the pH reached 7. Then, the oxidized cellulose fibers were filtered and washed using distilled water. To obtain a 2% (w/w) suspension of the water-insoluble oxidized cellulose, the suspension was added to 200 mL of distilled water. The suspension was then sonicated in an ice bath for 30 minutes at 10-minute intervals to prevent overheating. As a result, cellulose nanofibril suspensions were obtained.

2.3. Preparation of Ca-alginate-cellulose nanofibril beads.

Ca-alginate-cellulose nanofibril beads were prepared according to Benhouria et al. [16]. Alginate-cellulose nanofibril was dissolved in distilled water and stirred at room temperature until homogenous. The concentration percentages of cellulose nanofibrils at 40 mg/L of the polymeric matrix were 0, 5, 10, 15, and 20% for AC0, AC5, AC10, AC15, and AC20 composite

beads, respectively. The homogenous mixture was squeezed out through a syringe without a needle. After that, The mixture was carefully released from the syringe into a calcium chloride solution (4 % w/w, diluted in cold distilled water) under mild agitation. In this process, the soluble alginate-cellulose nanofibril was transformed into water-insoluble Ca-alginate-cellulose nanofibril beads by sodium chloride, which acts as an agent of crosslinking for alginate. The obtained beads were allowed to harden for 3 hours at room temperature. Lastly, the beads were filtered and washed several times with sterile water to remove the ionized calcium residue.

2.4. Characterization.

2.4.1. FTIR.

The powder from corncobs, isolated cellulose, and cellulose nanofibril was analyzed using a Bruker Alpha Infrared Spectrophotometer with a detector of RT-DLaTGS ZnSe. The experiments were measured in the range of 500–4000 cm^{-1} with a total of 24 scans for each sample.

2.4.2. Carboxylate content measurement.

A total of carboxylic groups in corncobs, isolated cellulose, and cellulose nanofibrils were measured using conductometric titration, described previously with minor modifications [17–19]. The suspensions with 0.05% solid content concentration were made with 80 mL of distilled water and 5 mL of 0.01 M NaCl. The solution of 0.1 M HCl was added dropwise until the pH of the suspensions was 2.5–3. A conductometer (Conductivity Probe-Vernier, USA) and magnetic stirring were used to measure conductivity. Then, the mixture suspensions were attached with a 0.01 M NaOH solution at 0.1 mL/min until the pH reached about 11. A NaOH solution was added to lower the conductivity and neutralize the acid. When the acid neutralization was complete (V1, mL), the conductivity remained constant until the endpoint (V2, mL) as the carboxylic group neutralization process. After that, the addition of a continuously prepared NaOH solution increased its conductivity. All measurements were carried out in duplicate. The carboxyl content was calculated using Equation 1.

$$mmol/g = \frac{M\ NaOH\ x\ (V_2 - V_1)}{weight\ of\ cellulose\ (g)} \tag{1}$$

2.4.3 Particle size, distribution, and zeta potential measurement.

The particle size, distribution, and zeta potential of 1% wt cellulose nanofibril suspension were analyzed by a nanoparticle size analyzer with a PMT detector at 90 degrees (HORIBA, Type SZ-100Z). The data of particle size obtained are presented in graph diameter versus frequency, and for distribution, particle size obtained graph diameter versus undersize. The zeta potential was recorded as a graph of zeta potential versus intensity.

2.4.4. Bead size range.

The size of the wet and dry beads from each formulation was measured using a micrometer screw (0.01 millimeters). The data was gathered and plotted against the diameter size of the beads.

2.4.5. Scanning electron microscope (SEM).

The topography of the beads with (AC20) and without (AC0) cellulose nanofibril was observed by SEM TM3030Plus Tabletop Microscope (Hitachi, China). At room temperature, the dried bead was placed in an adhesive carbon tip and evaluated with an accelerating voltage of 2-10 kV at magnifications of x100 and x1000.

2.4.6. Drying rate study of the beads.

The wet beads from various formulations were selected from several samples and weighed using an analytical balance until the mass was nearly equal. The beads were then dried in an oven at 30 °C until the mass was consistent. The masses of the beads were measured at 1-hour intervals. The experiment was performed three times to ensure repeatable results. The obtained average values were then used to plot mass against time.

2.4.7. Swelling properties.

The analytical balance was used to analyze the dried beads from three distinct formulations. The samples were then incubated at room temperature in distilled water. The hourly mass of three distinct beads from each formulation was measured, and the mean value was determined. This procedure included measuring the mass of the enlarged beads until they remained consistent. Using Equation 2, the percentage of swelling degree was computed. The experiment was evaluated three times.

$$\% \, swelling \, degree = \frac{(wet \, weight - dry \, weight)}{dry \, weight} x100 \tag{2}$$

3. Results and Discussion

3.1. Purification and chemical composition.

Cellulose is the largest component of plants, composed of lignin and hemicellulose. Corncobs are composed of 41% cellulose, 36% hemicellulose, 16% lignin, and 7% water content [20]. The pretreatment technique was used to separate non-cellulose chemicals in an effort to extract cellulose from corncobs, namely alkalization for delignification and bleaching [21], as shown in Figure 1. The corncobs in Figure 1b are prepared through a grinding process and then passed to a sieve with a size of 250 microns. Then, it was delignified using sodium hydroxide to dissolve lignin and hemicellulose compounds. It leads to a color change from yellow to blackish brown, as seen in Figure 1b. The delignification mechanism involved the saponification of structural ester bonds that bound xylane (hemicellulose) and lignin, which were then substituted into carboxylic salts and structures by nucleophilic acyls. As a result, lignin would be structurally separated from hemicellulose. Furthermore, lignin would be degraded by breaking the glycosidic bonds of the ether bond to produce ferulic acid and dissolved p-coumarin acid [22].

As illustrated in Figure 1c, bleaching with a 1.4% NaClO (v/v) solution was used to achieve pure cellulose. Compared to Figure 1b, the bleached cellulose powder product is lighter in hue and yields 50%. The bleaching method oxidizes and dissolves phenolic molecules or chromophore groups from lignin, producing white cellulose fibers [23].
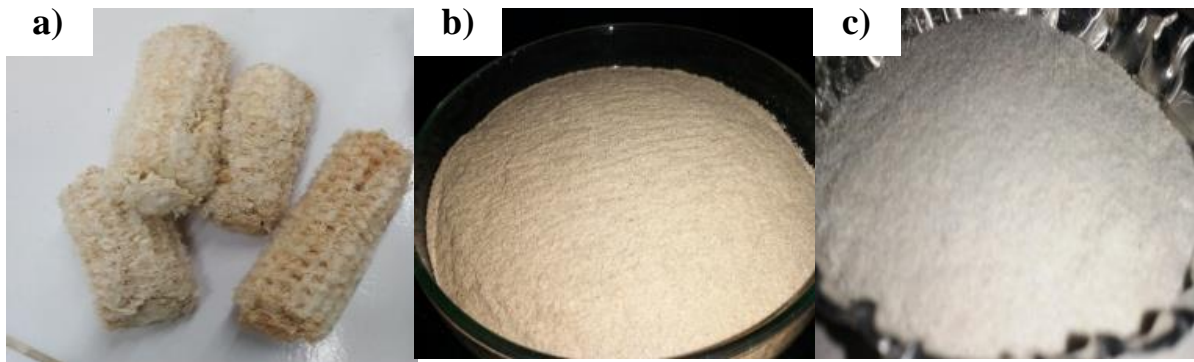
Figure 1. Cellulose product before and after purification: **(a)** ear corncobs, **(b)** cellulose delignification, and **(c)** cellulose powder product after the bleaching process.

Figure 2 reflects the infrared spectra of corncobs, isolated cellulose, and cellulose nanofibrils. All samples generally have typical absorbance peaks from cellulose, such as the band peaks in the region of 3300 cm⁻¹ and at 1100 cm⁻¹ that are assigned to OH stretching and OH bending, respectively. The CH_2 stretching frequency appeared as a small peak at 2925 cm⁻¹. The peak at 1100 cm⁻¹ is assigned to CO stretching, and the peak at 897 cm⁻¹ is attributed to the chemical bond of the cellulose chain's b-glycosidic linkage (C–O–C). In the spectra of corncobs, the peak at 1448 cm⁻¹ is indicated by the presence of lignin and is attributed to the vibration of skeletal C=C aromatics from the lignin structure [24–26]. However, the peak is significantly reduced in the spectra of isolated cellulose and cellulose nanofibrils because of the elimination of lignin by the delignification process using chemical treatments. The peak at 1100 cm⁻¹ appears in all the FTIR spectra that are assigned to the C-O-C asymmetric stretching of the lignin and hemicellulose structures. The broad peak at 1112 cm⁻¹ is assigned to the C-O-C linkage from lignin and hemicellulose.
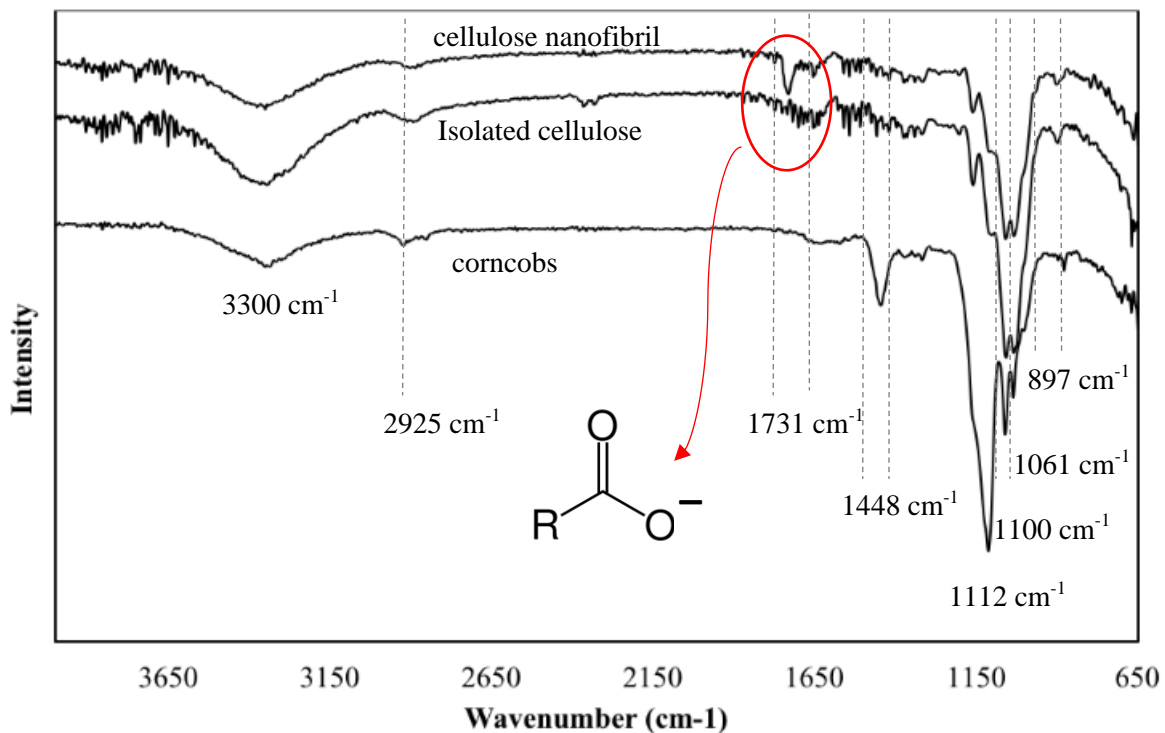

Figure 2. Spectrum IR of corncobs, isolated cellulose, and cellulose nanofibrils.

The intensity of these peaks is sharply reduced after chemical treatment due to the removal of the hemicellulose component [27]. The small peak at 1731 cm⁻¹, which appears only on the spectra of cellulose nanofibrils, is related to C=O vibration as a surface charge on

cellulose because of the oxidation reaction by TEMPO/NaBr/NaClO reagent that occurs in the extraction of cellulose nanofibrils, as reported in previous literature [17,28]. The peaks at 1061 and 897 cm^{-1} are assigned to the C-O stretching and the C-H rock vibrations of the cellulose [29], which appear in all spectra. The differences in all the spectra indicate that the cellulose nanofibril material has a higher purity of cellulose due to the reduced total of peaks that appear.

3.2. Mechanism of production of cellulose nanofibrils.

TEMPO-mediated oxidation leads to stable aqueous suspensions of cellulose nanofibril, which are negatively charged and do not tend to aggregate. During the oxidation process, the C6 primary hydroxyl group of cellulose fibrils was converted to the carboxylate group [17,30–32]. The production of stable cellulose nanofibril suspension from corncobs is shown in Figure 3.
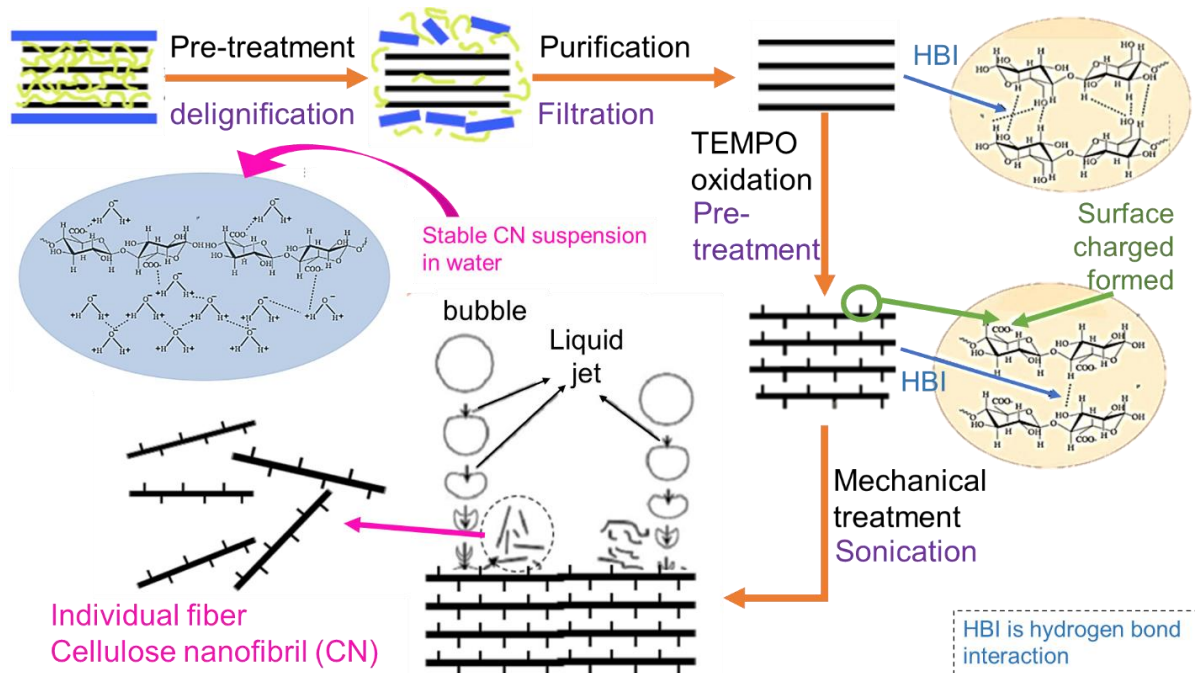
Figure 3. Schematic illustration of production cellulose nanofibril suspension from fibril cellulose.

The presence of the carboxyl groups in cellulose nanofibrils was confirmed by the FTIR, as seen in Figure 2. These carboxyl groups will form the surface charges on cellulose nanofibrils. The surface charges will cause intermolecular repulsion, making it easier to form individual fibers, followed by mechanical treatment [33]. The individual fibers of cellulose nanofibril will form a stable suspension in water.

The nano-size is important for cellulose nanofibril particles' stability and surface area. Thus, a particle size analyzer measured cellulose nanofibril suspensions' particle size and distribution, as shown in Figure 4. The average diameter of these fibers was 153,4 nm, and the value of the polydispersity index is 0.044, which is the nanofiber range [34]. These results are further evidence of the successful production of nanosized cellulose fibers in terms of length and width. Furthermore, the particle size distribution shows that the cellulose nanofibrils obtained from corncobs with TEMPO oxidation and mechanical treatment are relatively homogeneous.
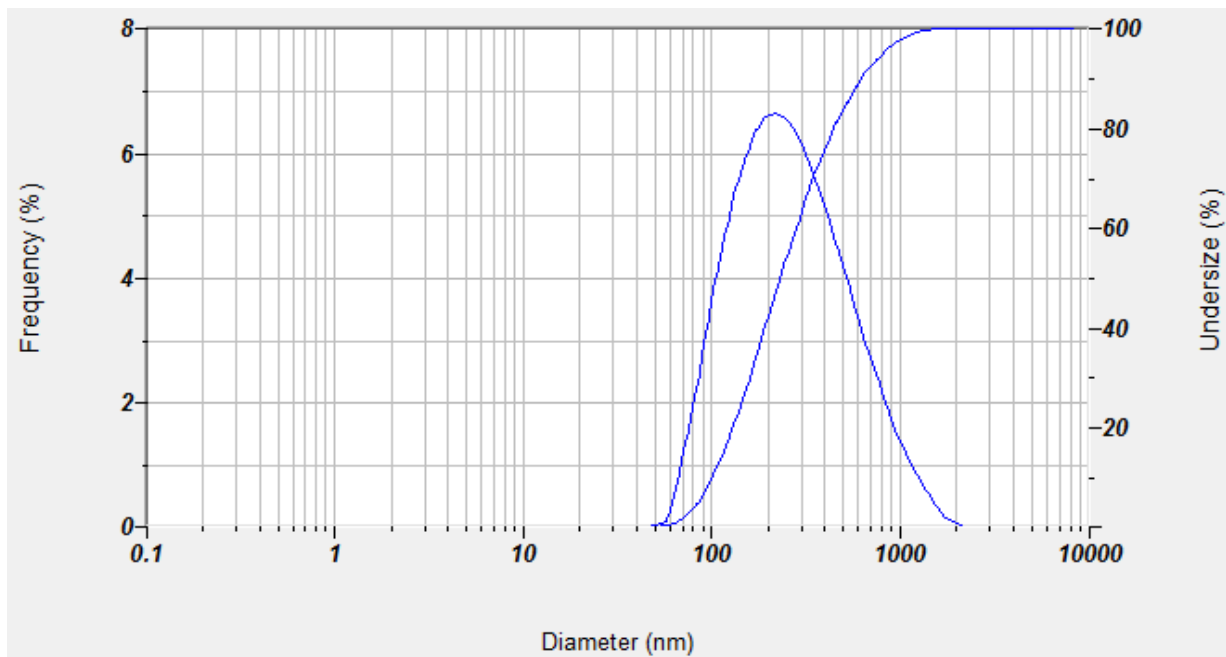
Figure 4. Particle size and distribution of cellulose nanofibrils suspensions.

The content of carboxyl groups was measured by titration conductometry according to the conductivity of the suspension sample. Figure 5a presents a graph of the conductivity correlation and volume addition of NaOH resulting from titration conductometry for corncobs, isolated cellulose, and cellulose nanofibrils. The result shows that the conductivity decreases gradually owing to the neutralization of an acid by the addition of NaOH (V_1). The conductivity remained constant during carboxyl group neutralization. At the end of the neutralization process (V_2), excess NaOH would increase the conductivity of suspense. Weak acids, such as carboxyl groups, affect the amount of NaOH required to neutralize carboxyl groups (V). The calculation using Eq.1 yields the carboxyl content value depicted in Figure 5b. The cellulose nanofibril has three times the carboxyl content of other materials. It suggested that TEMPO oxidation enhances the carboxyl group's presence on the cellulose nanofibril structure. The presence of even a modest quantity of carboxyl in corncobs and separated cellulose implies impurity [35].
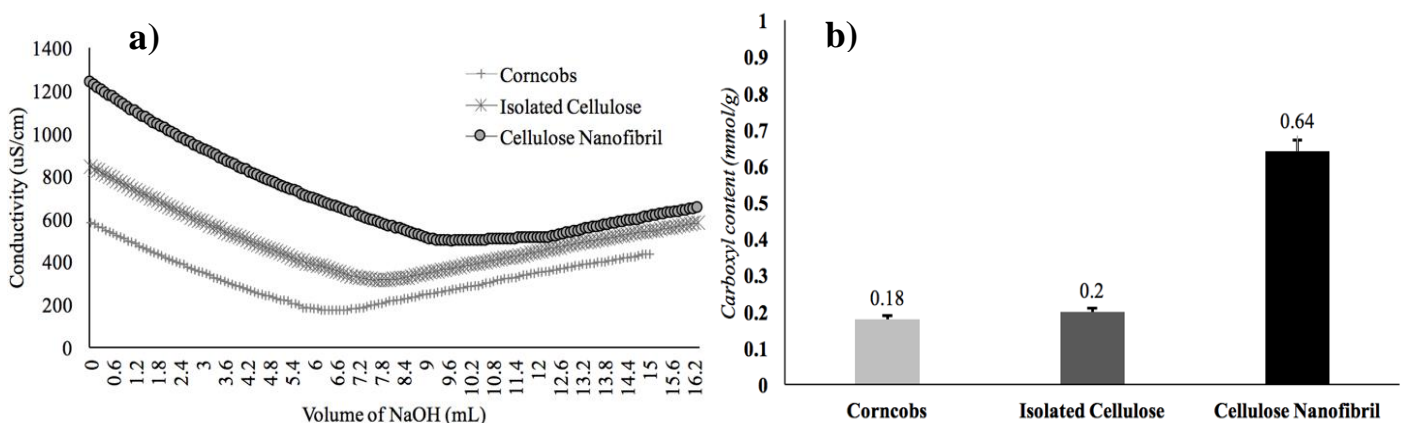

Figure 5. Graph titration conductometric **(a)** and carboxyl content **(b)** of corncobs, isolated cellulose, and cellulose nanofibril.

Surface charge is a critical characteristic affecting nanoparticle stability and diffusion rate. Thus, the electrical properties of cellulose nanofibril suspensions with good dispersibility

were measured by zeta potential. The mean zeta potential of cellulose nanofibril suspensions is -46.3 mV, as shown in Figure 6.
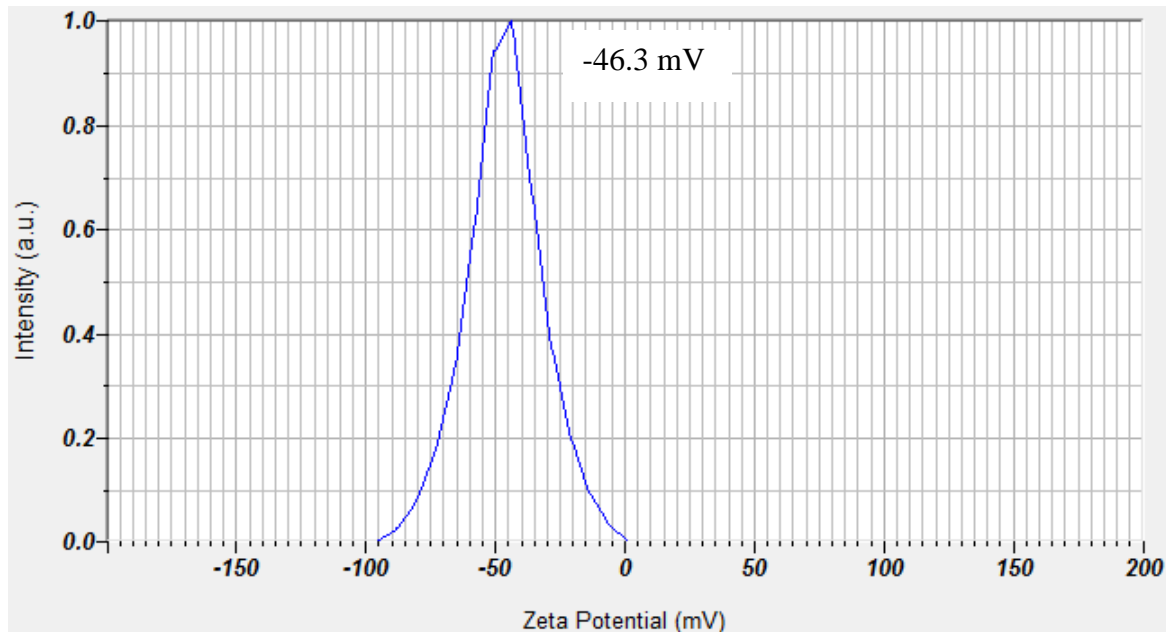
Figure 6. Profile graph of zeta potential of cellulose nanofibrils suspensions.

3.3. Beads composite with alginate.

Alginate is a naturally occurring polymer that can be used as an encapsulation agent with Ca^{2+} crosslinking [40]. In this study, cellulose nanofibril was added to the alginate solution to produce composite beads. To investigate the influence of cellulose nanofibril level, different cellulose nanofibril concentrations such as 5, 10, 15, and 20 wt.% were used to produce calcium alginate-cellulose nanofibril, which is named AC5, AC10, AC15, and AC20, respectively. The mixtures were dropped into the calcium chloride solution by syringe to form the beads due to the crosslinking of alginate and calcium ions, as shown in Figure 7.
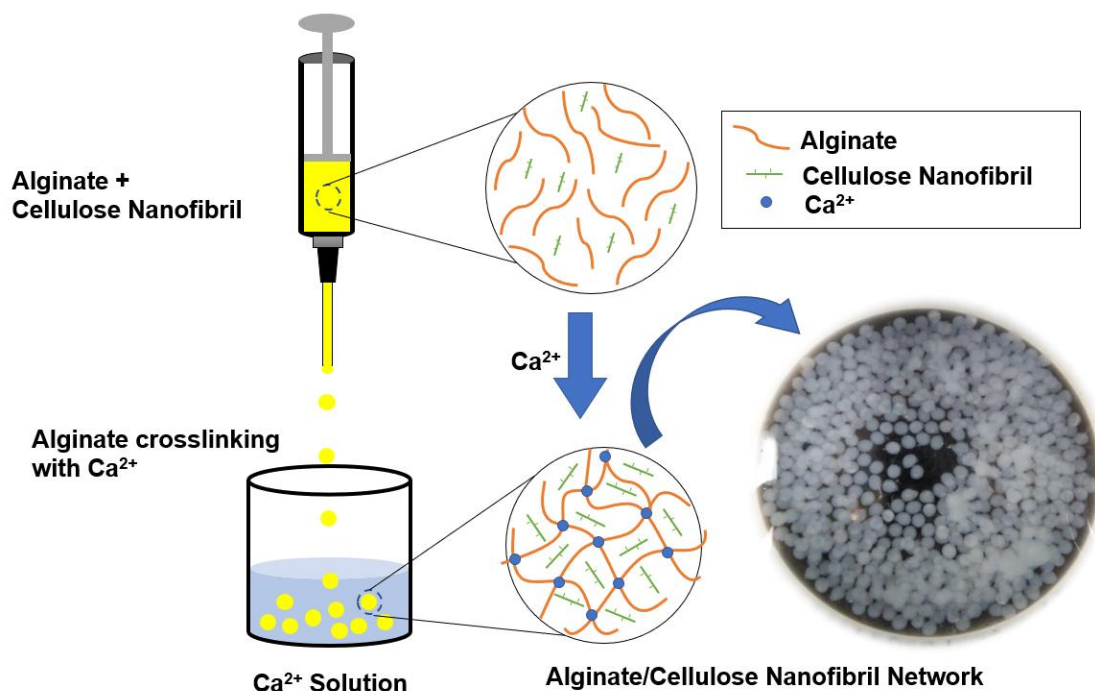
Figure 7. Crosslinking process for the production of alginate/cellulose nanofibrils beads composite.

This value is greater than the cellulose nanocrystal suspension reported by Niu *et al.* [36] of -43 mV after acid hydrolysis for 10 hours. Generally, suspension particles are stable when the absolute value of the zeta potential is higher than -30 mV [37,38]. These results show that the formation of carboxyl groups as a surface charge contributes to the increase of the zeta potential of cellulose nanofibril suspensions and improves the stability and dispersibility of the cellulose nanofibril particles. The stability and dispersibility of nanocellulose particles were maintained due to the electrostatic interactions caused by the small size of the nanocellulose particles and the higher zeta potential, resulting in a more stable suspension [39].

Figure 8 depicts the diameter sizes of wet and dry beads of different compositions and then inserts photographs of AC0 beads (without cellulose nanofibril) and AC20 beads (with cellulose nanofibril). The results show that the presence of cellulose nanofibril reduced the diameter of the beads. The presence of surface charge in the cellulose nanofibril causes alginate-cellulose nanofibril bonds to become stronger, resulting in a smaller diameter of the wet beads due to shrinking [41]. While the dry beads demonstrate slight differences in all compositions, increasing the cellulose nanofibril concentration in the beads slightly reduced the diameter of the beads. It is noted that the concentration of cellulose nanofibril did not significantly affect the diameter size of the beads. Indeed, by a slight addition, the diameter size of the beads was reduced. These results are similar to the previous study [14,41,42] with the use of cellulose nanocrystals as filler in a composite of Poly Vinyl Alcohol (PVA) film. The result describes that the presence of the cellulose nanocrystal in the PVA composites makes their mechanical properties better because of a close association between filler and matrix, possibly in which the hydrogen bond between cellulose nanocrystal and PVA forms.
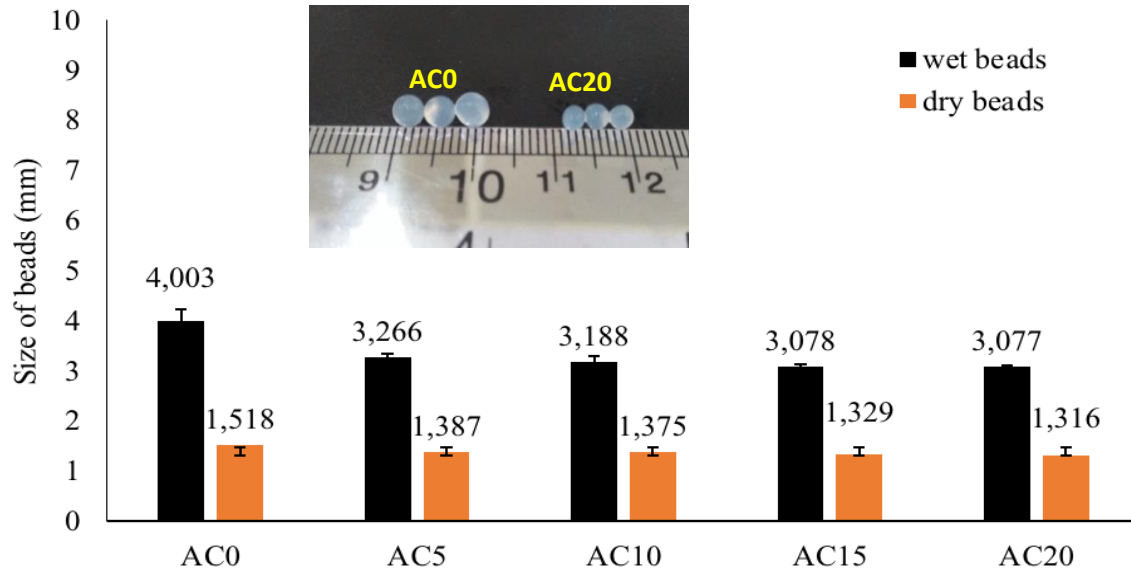
Figure 8. The diameter size of beads from different compositions, it was inserted in a photograph of wet beads AC0 and AC20.

3.4. Morphology of beads.

Figure 9 shows the morphology of beads by scanning electron microscopy without (AC0) and with (AC20) cellulose nanofibrils in their composition. AC20 beads have a smoother and more compact surface than AC0 beads (compared to Figures 9-a and 9-b). The density of AC20 beads is higher than AC0 beads under magnifications up to 1000x (Figures 9-a1 and 9-b1). The presence of cellulose nanofibril in the beads stimulates extensive

intermolecular interactions with the alginate structure [14,43]. The interaction of hydrogen bonds that occurs between alginate and cellulose nanofibrils increases density. Thus, the surface of the AC20 bead is more compact.
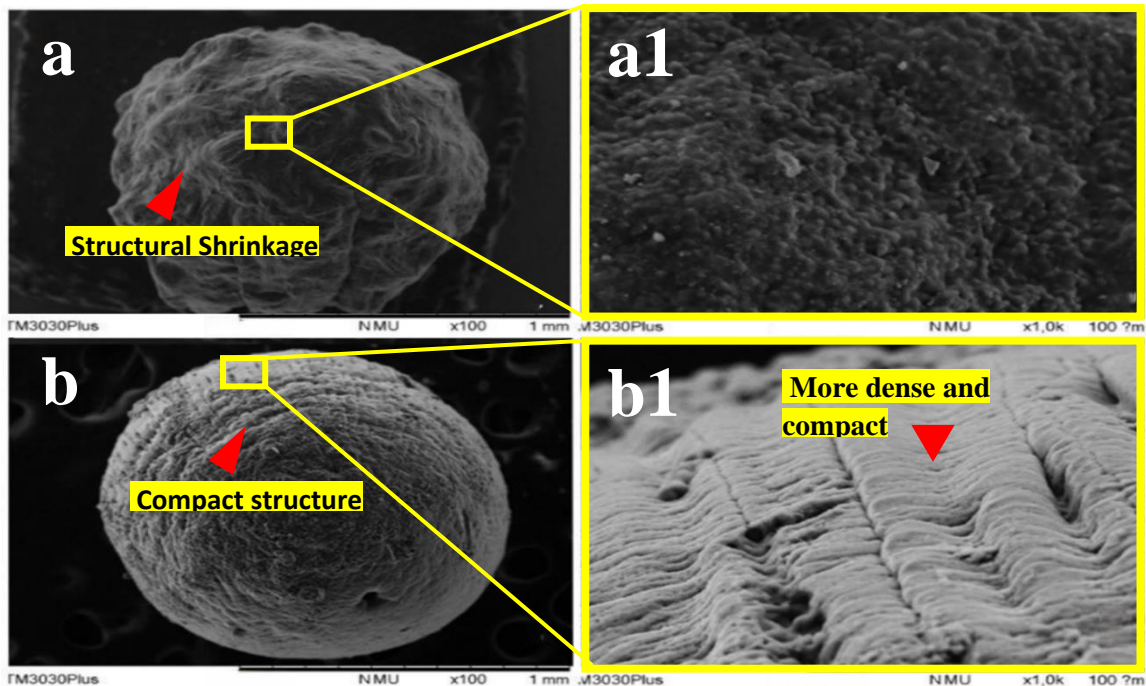
Figure 9. Image SEM of **(a)** AC0 and **(b)** AC20 formed beads with **(a1)** mag x100 and **(b1)** mag x1000.

3.5. Physical properties of the beads.

3.5.1. Effect of cellulose nanofibril concentration on drying beads.

The diffusion coefficients for the desorption of the liquid from the beads influenced the drying rate of the beads. Beads with different compositions were selected in such a way that the initial weight was almost equal.
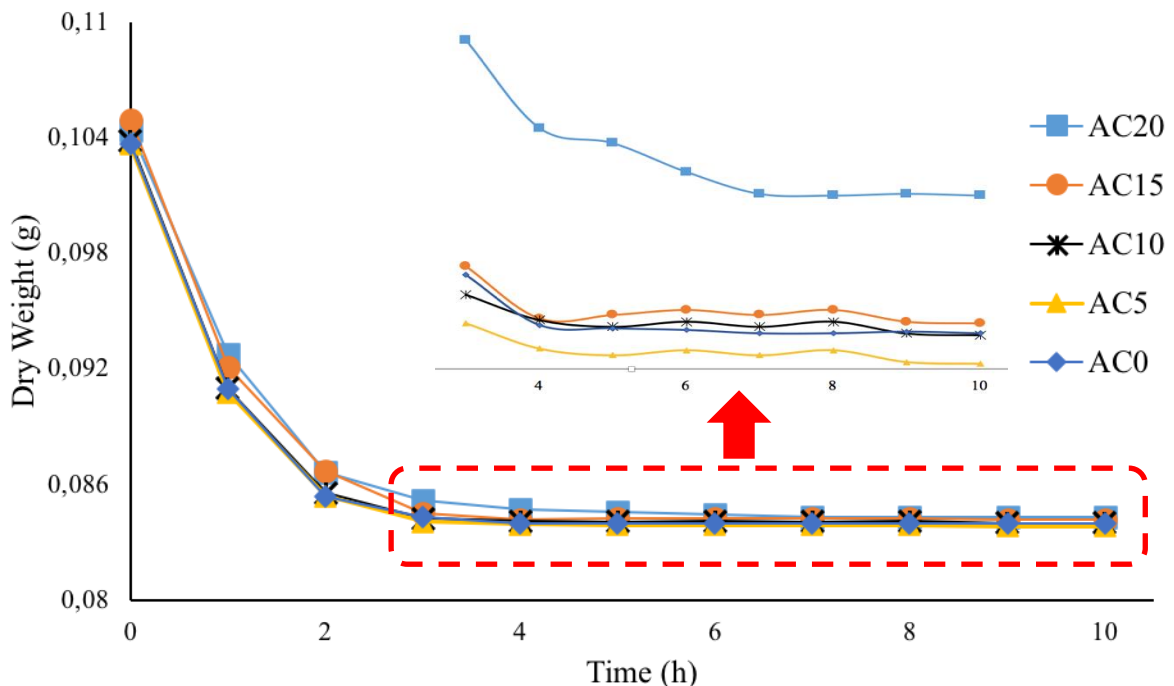
Figure 10. Effect varying composition of the beads on drying rate, it was inserted the graph scale time 3-10 h.

In this work, the effect of the cellulose nanofibril concentration in the beads on the drying rate is reflected in Figure 10. All bead samples show the same trends and state the exact times. Most bead samples determined a constant weight at the 4th hour, as seen in the picture range of 3–10 hours. However, the weight of the beads decreases as the amount of cellulose in the beads decreases. It was discovered that alginate beads containing less cellulose nanofibril and more water had a lower weight after drying than alginate beads containing more cellulose (AC20). The cellulose nanofibrils can interact strongly with alginate [14], making the matrix denser and more compact. Consequently, it minimizes the space available to bind water.

3.5.2. The Effect of cellulose nanofibril concentration on the water uptake.

The effects of the cellulose nanofibril concentration on the percentage of water uptake by the beads of different compositions were also evaluated. Figure 11 depicts the relationship between swelling degree percentage and time soaking. The beads showed the maximum water uptake during the first hour. According to the results, AC0 (without cellulose nanofibril) beads have a higher swelling than the beads containing cellulose nanofibril. AC0 beads have a greater capacity for water uptake than cellulose nanofibril beads. The presence of hydroxyl and carboxyl groups in the cellulose nanofibril structure reduces water uptake. In addition, the enhancement of cellulose nanofibril concentration will slightly reduce the hydration degree of the beads. For instance, AC0 decreased from 255% to 203%. It might be due to the increased physical crosslinking and reduced porosity in the beads [44]. The presence of carboxyl groups as surface charges and hydroxyl groups in cellulose nanofibrils will provide strong intermolecular interactions in a polymeric alginate matrix, resulting in increased bead density and decreased diameter size [45]. The increasing density of the beads will limit the matrix space for water uptake, so the swelling degree was decreased.
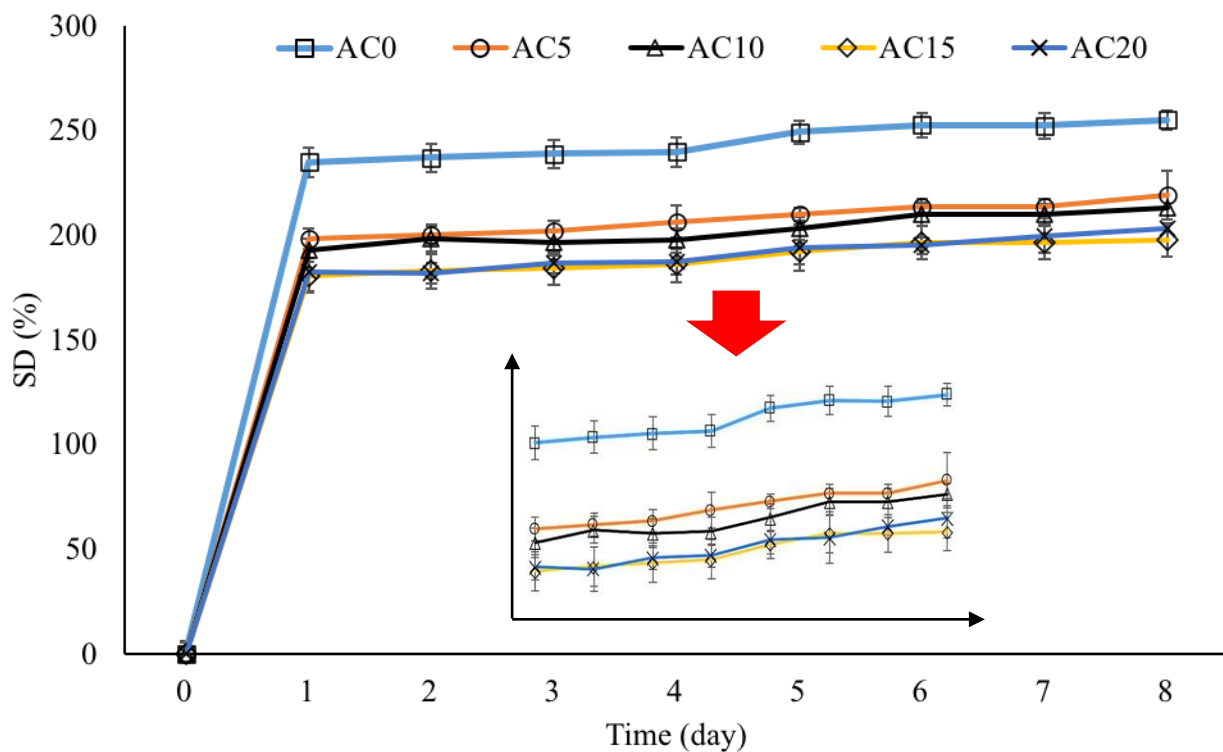
Figure 11. Percentage of the swelling degree of the beads from all formulations.

3.6. Swelling kinetics.

The swelling behavior of bead composites plays an important role in obtaining good properties, especially in protecting the encapsulation and slow-release bioactive. To investigate the kinetic model above for the bead composite, the graph is t versus t/s, as shown in Figure 12a, and we can get the values of *ri* (the initial level of swelling), *ks* (the swelling rate constant), and *Seq* (theoretical equilibrium) from the slope and intersection of the plotted lines, as shown in Table 1. The bead swelling mechanism can be determined using Equation 3.

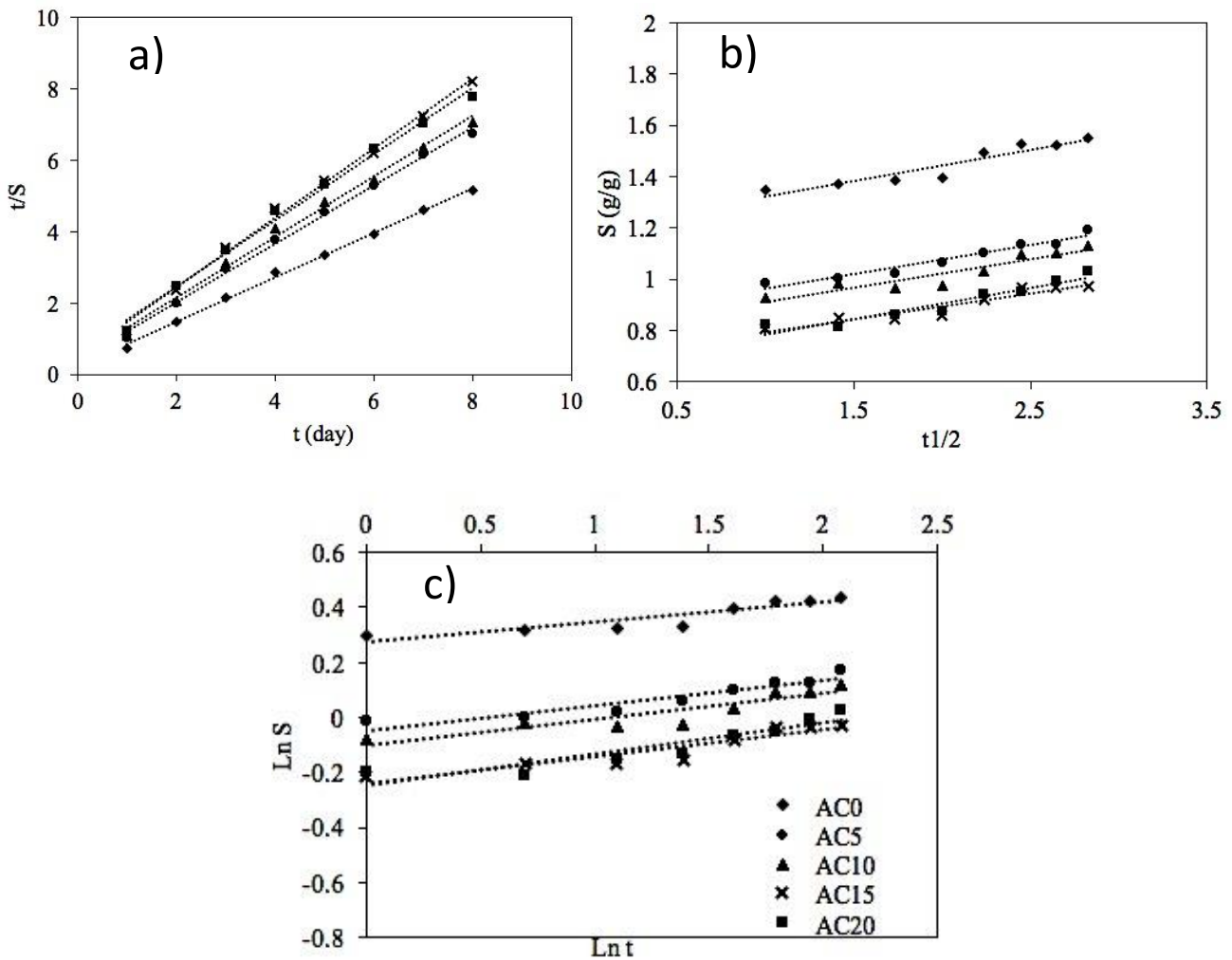$$swelling \ ratio \ (S) = \left(\frac{Ws - Wd}{Wd}\right) = kt^n \tag{3}$$

where *S* is the fractional swelling ratio at time *t,* Ws is the swollen bead weight at time t, and Wd is the dried bead weight at time t = 0. The parameters for the water transport mechanism are *k* and *n, which* are the swelling constant and the swelling exponent, respectively [46,47]. The value of the swelling exponent (*n*) can be obtained from the slope of the drawn *ln t* versus *ln S,* and this value result can identify the diffusion mechanism. According to the literature [48], when n ≤ 0.5, the diffusion mechanism is Fickian diffusion, and when 0.5 < n < 1.0, the diffusion mechanism is non-Fickian diffusion or anomalous diffusion. But, when *n = 1*, the diffusion mechanism is indicated as Case II diffusion, and when *n* > 1, it is called a super Case II diffusion mechanism, which is rarely possible. The values of *n* and *k,* as shown in Table 1, are obtained from the slope and intercept plotted in Figure 12c. The developed bead composite shows a Fickian-type diffusion mechanism, which is more suitable for biomedical applications such as drug delivery control and bioactive encapsulation. The swelling constant (*k*) can be associated with the diffusion coefficient (*D*) for Fickian diffusion [49]. The swelling ratio equation of the beads can be used in Equation 4.

$$S = \sqrt{\frac{D}{\pi r^2}} \sqrt{t} \tag{4}$$

where *D* is the diffusion coefficient of the bead, *r* is the radius of the bead, *S* is the swelling ratio, and *t* is the time that refers to a diffusion length. The value of *D* was obtained from the slope of the line plot drawn from $t^{1/2}$ versus *S,* as shown in Figure 12b. The result shows that the D value of AC0 is 0.1089 $mm^2.d^{-1}$, AC5 is 0.0779 $mm^2.d^{-1}$, AC10 is 0.0747 $mm^2.d^{-1}$, AC15 is 0.0558 $mm^2.d^{-1}$, and AC20 is 0.0805 $mm^2.d^{-1}$, indicating that the enhanced concentration of cellulose nanofibrils in the beads makes for a slow diffusion rate of the molecules. The lower water diffusion might be associated with the presence of cellulose nanofibrils in the matrix network. Further, as the concentration increased, the water uptake capacity of the prepared beads improved. Table 1 shows the kinetic parameters obtained.

Table 1. Swelling kinetic parameters of beads composite

Beads Code	Swelling Exponent (*n*)	Diffusion Coefficient (*D*) $mm^2.s^{-1}$	Initial Swelling Rate (*ri*) [g water/g beads]/day	Theoretical Equilibrium Swelling (*Seq*) [g water/g beads]	Swelling Rate Constant (*ks*) [g beads/g water/ day]
AC0	0.0730	0.1089	0.2250	1.6013	1.7333
AC5	0.0909	0.0779	0.3772	2.6511	0.3772
AC10	0.0936	0.0747	0.4325	2.3121	0.4325
AC15	0.0972	0.0558	0.4732	2.1133	0.4732
AC20	0.1137	0.0805	0.5958	1.6784	0.5958

Figure 12. Swelling kinetics curves of beads in water: **(a)** t/s versus t curves, **(b)** Ln S versus Ln t, and **(c)** swelling ratio versus $t^{1/2}$ curves.

4. Conclusions

This study demonstrated that cellulose nanofibrils were successfully extracted from corncobs by a simple technique using alkali and sodium chlorite. The oxidation by TEMPO-mediated and mechanical ultrasonication led to the production of stable aqueous suspensions of cellulose nanofibrils, which are negatively charged because of the presence of carboxyl groups. The resulting cellulose nanofibrils were exhibited in a stable water solution (-46.3 mV) with particle sizes in the nanoscale range (56 nm). At various concentrations of cellulose nanofibrils, the size of the alginate-cellulose nanofibrils beads dropped by 4.003, 3.266, 3.188, 3.078, and 3.077 mm for 0, 5, 10, 15, and 20% of cellulose nanofibrils, respectively. The morphology of the beads with cellulose nanofibrils (AC20) is denser and more compact than without cellulose nanofibrils (AC0). Enhancing the cellulose nanofibrils in the bead reduced water absorption from 255% in the AC0 beads to 203% in the AC20 beads. A Fickian-type diffusion mechanism identifies the behavior of the beads with diffusion rates of 0.0558 and 0.1089 $mm^2 d^{-1}$ for AC15 and AC0, respectively. These improvements in physical properties suggest a strong interaction between alginate and cellulose nanofibrils due to the hydrogen bond and presence of carboxyl groups, indicating a high potential for their use as filler agents in the matrix of nanocomposites, particularly for encapsulating bioactive materials.

Funding

Acknowledgments

Conflicts of Interest

The authors declare no conflict of interest.

References

1. Vijian, R.S.; Yusefi, M.; Shameli, K. Plant Extract Loaded Sodium Alginate Nanocomposites for Biomedical Applications: A Review. *J. Res. Nanosci. Nanotechnol.* **2022**, *6*, 14–30, https://doi.org/10.37934/JRNN.6.1.1430.
2. Kaushalya, K.G.D.; Gunathilake, K.D.P.P. Encapsulation of Phlorotannins from Edible Brown Seaweed in Chitosan: Effect of Fortification on Bioactivity and Stability in Functional Foods. *Food Chem.* **2022**, *377*, 132012, https://doi.org/10.1016/J.FOODCHEM.2021.132012.
3. Vučurović, V.M.; Puškaš, V.S.; Miljić, U.D. Bioethanol Production from Sugar Beet Molasses and Thick Juice by Free and Immobilised Saccharomyces Cerevisiae. *J. Inst. Brew.* **2019**, *125*, 134–142, https://doi.org/10.1002/JIB.536.
4. Liu, C.; Ye, J.; Lin, Y.; Wu, J.; Price, G.W.; Burton, D.; Wang, Y. Removal of Cadmium (II) Using Water Hyacinth (Eichhornia Crassipes) Biochar Alginate Beads in Aqueous Solutions. *Environ. Pollut.* **2020**, *264*, 114785, https://doi.org/10.1016/J.ENVPOL.2020.114785.
5. Azad, A.K.; Al-Mahmood, S.M.A.; Chatterjee, B.; Wan Sulaiman, W.M.A.; Elsayed, T.M.; Doolaanea, A.A. Encapsulation of Black Seed Oil in Alginate Beads as a PH-Sensitive Carrier for Intestine-Targeted Drug Delivery: *In vitro*, *In vivo* and Ex Vivo Study. *Pharm. 2020, Vol. 12, Page 219* **2020**, *12*, 219, https://doi.org/10.3390/PHARMACEUTICS12030219.
6. Ahmad Raus, R.; Wan Nawawi, W.M.F.; Nasaruddin, R.R. Alginate and Alginate Composites for Biomedical Applications. *Asian J. Pharm. Sci.* **2021**, *16*, 280–306, https://doi.org/10.1016/J.AJPS.2020.10.001.
7. Batista, D.P.C.; De Oliveira, I.N.; Ribeiro, A.R.B.; Fonseca, E.J.S.; Santos-Magalhães, N.S.; De Sena-Filho, J.G.; Teodoro, A. V.; Grillo, L.A.M.; De Almeida, R.S.; Dornelas, C.B. Encapsulation and Release of Beauveria Bassiana from Alginate–Bentonite Nanocomposite. *RSC Adv.* **2017**, *7*, 26468–26477, https://doi.org/10.1039/C7RA02185B.
8. Kim, J.; Hlaing, S.P.; Lee, J.; Saparbayeva, A.; Kim, S.; Hwang, D.S.; Lee, E.H.; Yoon, I.S.; Yun, H.; Kim, M.S.; *et al*. Exfoliated Bentonite/Alginate Nanocomposite Hydrogel Enhances Intestinal Delivery of Probiotics by Resistance to Gastric PH and on-Demand Disintegration. *Carbohydr. Polym.* **2021**, *272*, 118462, https://doi.org/10.1016/J.CARBPOL.2021.118462.
9. Gowri, M.; Latha, N.; Suganya, K.; Kumar, S.K.; Alahmadi, T.A.; Alharbi, S.A.; Murugan, M.; Rajan, M. Amoxicillin Loaded Nickel Functionalized Polymeric Bentonite Carrier for Enhanced Therapeutic Activity. *J. Polym. Res.* **2020**, *27*, 1–12, https://link.springer.com/article/10.1007/s10965-020-02340-w.
10. Lupașcu, R.E.; Ghica, M.V.; Dinu-Pîrvu, C.E.; Popa, L.; Velescu, B. Ștefan; Arsene, A.L. An Overview Regarding Microbial Aspects of Production and Applications of Bacterial Cellulose. *Mater. 2022, Vol. 15, Page 676* **2022**, *15*, 676, https://doi.org/10.3390/MA15020676.
11. Ramadhani, D.V.; Holilah, H.; Bahruji, H.; Jadid, N.; Oetami, T.P.; Jalil, A.A.; Asranudin, A.; Ediati, R.; Masruchin, N.; Suryanegara, L.; *et al*. Effect of Lignocellulosic Composition of Reutealis Trisperma Waste on Nanocrystalline Cellulose Properties. *Biocatal. Agric. Biotechnol.* **2022**, *45*, 102516, https://doi.org/10.1016/J.BCAB.2022.102516.
12. Yi, T.; Zhao, H.; Mo, Q.; Pan, D.; Liu, Y.; Huang, L.; Xu, H.; Hu, B.; Song, H. From Cellulose to Cellulose Nanofibrils—A Comprehensive Review of the Preparation and Modification of Cellulose Nanofibrils. *Mater. 2020, Vol. 13, Page 5062* **2020**, *13*, 5062, https://doi.org/10.3390/MA13225062.
13. Xu, H.; Sanchez-Salvador, J.L.; Balea, A.; Blanco, A.; Negro, C. Optimization of Reagent Consumption in TEMPO-Mediated Oxidation of Eucalypt Cellulose to Obtain Cellulose Nanofibers. *Cellulose* **2022**, *29*, 6611–6627, https://link.springer.com/article/10.1007/s10570-022-04672-w.
14. Silvério, H.A.; Flauzino Neto, W.P.; Dantas, N.O.; Pasquini, D. Extraction and Characterization of Cellulose Nanocrystals from Corncob for Application as Reinforcing Agent in Nanocomposites. *Ind. Crops Prod.* **2013**,

44, 427–436, https://doi.org/10.1016/J.INDCROP.2012.10.014.

15. Masruchin, N.; Amanda, P.; Kusumaningrum, W.B.; Suryanegara, L.; Nuryawan, A. Particle Size Distribution and Yield Analysis of Different Charged Cellulose Nanofibrils Obtained by TEMPO-Mediated Oxidation. *IOP Conf. Ser. Earth Environ. Sci.* **2020**, *572*, 012045, https://doi.org/10.1088/1755-1315/572/1/012045.

16. Benhouria, A.; Islam, M.A.; Zaghouane-Boudiaf, H.; Boutahala, M.; Hameed, B.H. Calcium Alginate–Bentonite–Activated Carbon Composite Beads as Highly Effective Adsorbent for Methylene Blue. *Chem. Eng. J.* **2015**, *270*, 621–630, https://doi.org/10.1016/J.CEJ.2015.02.030.

17. Masruchin, N.; Park, B.D.; Causin, V.; Um, I.C. Characteristics of TEMPO-Oxidized Cellulose Fibril-Based Hydrogels Induced by Cationic Ions and Their Properties. *Cellulose* **2015**, *22*, 1993–2010, https://link.springer.com/article/10.1007/s10570-015-0624-0.

18. Beck, S.; Méthot, M.; Bouchard, J. General Procedure for Determining Cellulose Nanocrystal Sulfate Half-Ester Content by Conductometric Titration. *Cellulose* **2015**, *22*, 101–116, https://link.springer.com/article/10.1007/s10570-014-0513-y.

19. Abitbol, T.; Kloser, E.; Gray, D.G. Estimation of the Surface Sulfur Content of Cellulose Nanocrystals Prepared by Sulfuric Acid Hydrolysis. *Cellulose* **2013**, *20*, 785–794, https://link.springer.com/article/10.1007/s10570-013-9871-0.

20. Winarsih, S.; Siskawardani, D.D. Hydrolysis of Corncobs Using a Mixture of Crude Enzymes from Trichoderma Reesei and Aspergillus Niger for Bioethanol Production. *Energy Reports* **2020**, *6*, 256–262, https://doi.org/10.1016/J.EGYR.2020.11.141.

21. Holilah, H.; Prasetyoko, D.; Ediati, R.; Bahruji, H.; Jalil, A.A.; Asranudin, A.; Anggraini, S.D. Hydrothermal Assisted Isolation of Microcrystalline Cellulose from Pepper (Piper Nigrum L.) Processing Waste for Making Sustainable Bio-Composite. *J. Clean. Prod.* **2021**, *305*, 127229, https://doi.org/10.1016/J.JCLEPRO.2021.127229.

22. Wu, Z.; Peng, K.; Zhang, Y.; Wang, M.; Yong, C.; Chen, L.; Qu, P.; Huang, H.; Sun, E.; Pan, M. Lignocellulose Dissociation with Biological Pretreatment towards the Biochemical Platform: A Review. *Mater. Today Bio* **2022**, *16*, 100445, https://doi.org/10.1016/J.MTBIO.2022.100445.

23. Ditzel, F.I.; Prestes, E.; Carvalho, B.M.; Demiate, I.M.; Pinheiro, L.A. Nanocrystalline Cellulose Extracted from Pine Wood and Corncob. *Carbohydr. Polym.* **2017**, *157*, 1577–1585, https://doi.org/10.1016/J.CARBPOL.2016.11.036.

24. Sun, X.F.; Xu, F.; Sun, R.C.; Fowler, P.; Baird, M.S. Characteristics of Degraded Cellulose Obtained from Steam-Exploded Wheat Straw. *Carbohydr. Res.* **2005**, *340*, 97–106, https://doi.org/10.1016/J.CARRES.2004.10.022.

25. Cherian, B.M.; Pothan, L.A.; Nguyen-Chung, T.; Mennig, G.; Kottaisamy, M.; Thomas, S. A Novel Method for the Synthesis of Cellulose Nanofibril Whiskers from Banana Fibers and Characterization. *J. Agric. Food Chem.* **2008**, *56*, 5617–5627, https://doi.org/10.1021/jf8003674.

26. Saratale, R.G.; Cho, S.K.; Saratale, G.D.; Kadam, A.A.; Ghodake, G.S.; Magotra, V.K.; Kumar, M.; Bharagava, R.N.; Varjani, S.; Palem, R.R.; *et al*. Lignin-Mediated Silver Nanoparticle Synthesis for Photocatalytic Degradation of Reactive Yellow 4G and *In vitro* Assessment of Antioxidant, Antidiabetic, and Antibacterial Activities. *Polym. 2022, Vol. 14, Page 648* **2022**, *14*, 648, https://doi.org/10.3390/POLYM14030648.

27. Rosa, M.F.; Medeiros, E.S.; Malmonge, J.A.; Gregorski, K.S.; Wood, D.F.; Mattoso, L.H.C.; Glenn, G.; Orts, W.J.; Imam, S.H. Cellulose Nanowhiskers from Coconut Husk Fibers: Effect of Preparation Conditions on Their Thermal and Morphological Behavior. *Carbohydr. Polym.* **2010**, *81*, 83–92, https://doi.org/10.1016/J.CARBPOL.2010.01.059.

28. Barbash, V.A.; Yashchenko, O. V.; Gondovska, A.S.; Deykun, I.M. Preparation and Characterization of Nanocellulose Obtained by TEMPO-Mediated Oxidation of Organosolv Pulp from Reed Stalks. *Appl. Nanosci.* **2022**, *12*, 835–848, https://link.springer.com/article/10.1007/s13204-021-01749-z.

29. Alemdar, A.; Sain, M. Isolation and Characterization of Nanofibers from Agricultural Residues – Wheat Straw and Soy Hulls. *Bioresour. Technol.* **2008**, *99*, 1664–1671, https://doi.org/10.1016/J.BIORTECH.2007.04.029.

30. Guan, Q.; Chen, J.; Chen, D.; Chai, X.; He, L.; Peng, L.; Zhang, J.; Li, J. A New Sight on the Catalytic Oxidation Kinetic Behaviors of Bamboo Cellulose Fibers under TEMPO-Oxidized System: The Fate of Carboxyl Groups in Treated Pulps. *J. Catal.* **2019**, *370*, 304–309, https://doi.org/10.1016/J.JCAT.2019.01.003.

31. Duceac, I.A.; Tanasa, F.; Coseri, S. Selective Oxidation of Cellulose—A Multitask Platform with Significant Environmental Impact. *Mater. 2022, Vol. 15, Page 5076* **2022**, *15*, 5076, https://doi.org/10.3390/MA15145076.

32. Uusi-Tarkka, E.K.; Levanič, J.; Heräjärvi, H.; Kadi, N.; Skrifvars, M.; Haapala, A. All-Cellulose Composite Laminates Made from Wood-Based Textiles: Effects of Process Conditions and the Addition of TEMPO-Oxidized Nanocellulose. *Polym. 2022, Vol. 14, Page 3959* **2022**, *14*, 3959, https://doi.org/10.3390/POLYM14193959.

33. Woo, H.J.; Kim, J.H. Preparation of Nanofibrillated Cellulose and Its Effect on the Properties of PVA

Composite Film. *Polym.* **2018**, *42*, 52–58, https://doi.org/10.7317/PK.2018.42.1.52.

34. Asrofi, M.; Abral, H.; Kasim, A.; Pratoto, A.; Mahardika, M.; Park, J.W.; Kim, H.J. Isolation of Nanocellulose from Water Hyacinth Fiber (WHF) Produced via Digester-Sonication and Its Characterization. *Fibers Polym.* **2018**, *19*, 1618–1625, https://link.springer.com/article/10.1007/s12221-018-7953-1.

35. Pratama, A.W.; Piluharto, B.; Indarti, D.; Haryati, T.; Addy, H.S. Effect of Acid Concentration on Physical Properties and Surface Charge of Modified Cellulose. *ALCHEMY J. Penelit. Kim.* **2019**, *15*, 315–328, https://doi.org/10.20961/ALCHEMY.15.2.33756.315-328.

36. Niu, F.; Li, M.; Huang, Q.; Zhang, X.; Pan, W.; Yang, J.; Li, J. The Characteristic and Dispersion Stability of Nanocellulose Produced by Mixed Acid Hydrolysis and Ultrasonic Assistance. *Carbohydr. Polym.* **2017**, *165*, 197–204, https://doi.org/10.1016/J.CARBPOL.2017.02.048.

37. Javidi, F.; Razavi, S.M.A.; Mohammad Amini, A. Cornstarch Nanocrystals as a Potential Fat Replacer in Reduced Fat O/W Emulsions: A Rheological and Physical Study. *Food Hydrocoll.* **2019**, *90*, 172–181, https://doi.org/10.1016/J.FOODHYD.2018.12.003.

38. Silva, H.D.; Cerqueira, M.Â.; Vicente, A.A. Nanoemulsions for Food Applications: Development and Characterization. *Food Bioprocess Technol.* **2012**, *5*, 854–867, https://link.springer.com/article/10.1007/s11947-011-0683-7.

39. Whba Universiti Kebangsaan Malaysia Faizal Mohamed, F.; Kebangsaan Malaysia Mohd Syukri Yahya, U. Characterization of Cellulose Nanocrystalline (CNCs) Derived from Microcrystalline Cellulose (MCC) Synthesized Using Acid Hydrolysis Method. **2022**, https://doi.org/10.21203/RS.3.RS-2078344/V1.

40. Morozkina, S.; Strekalovskaya, U.; Vanina, A.; Snetkov, P.; Krasichkov, A.; Polyakova, V.; Uspenskaya, M. The Fabrication of Alginate–Carboxymethyl Cellulose-Based Composites and Drug Release Profiles. *Polym. 2022, Vol. 14, Page 3604* **2022**, *14*, 3604, https://doi.org/10.3390/POLYM14173604.

41. Spagnol, C.; Fragal, E.H.; Witt, M.A.; Follmann, H.D.M.; Silva, R.; Rubira, A.F. Mechanically Improved Polyvinyl Alcohol-Composite Films Using Modified Cellulose Nanowhiskers as Nano-Reinforcement. *Carbohydr. Polym.* **2018**, *191*, 25–34, https://doi.org/10.1016/J.CARBPOL.2018.03.001.

42. El Miri, N.; Abdelouahdi, K.; Zahouily, M.; Fihri, A.; Barakat, A.; Solhy, A.; El Achaby, M. Bio-Nanocomposite Films Based on Cellulose Nanocrystals Filled Polyvinyl Alcohol/Chitosan Polymer Blend. *J. Appl. Polym. Sci.* **2015**, *132*, https://doi.org/10.1002/APP.42004.

43. Supramaniam, J.; Adnan, R.; Mohd Kaus, N.H.; Bushra, R. Magnetic Nanocellulose Alginate Hydrogel Beads as Potential Drug Delivery System. *Int. J. Biol. Macromol.* **2018**, *118*, 640–648, https://doi.org/10.1016/J.IJBIOMAC.2018.06.043.

44. Jayaramudu, T.; Ko, H.U.; Kim, H.C.; Kim, J.W.; Kim, J. Swelling Behavior of Polyacrylamide–Cellulose Nanocrystal Hydrogels: Swelling Kinetics, Temperature, and PH Effects. *Mater. 2019,. 12, Page 2080* **2019**, *12*, 2080, https://doi.org/10.3390/MA12132080.

45. Correia, D.M.; Lizundia, E.; Fernandes, L.C.; Costa, C.M.; Lanceros-Méndez, S. Influence of Cellulose Nanocrystal Surface Functionalization on the Bending Response of Cellulose Nanocrystal/Ionic Liquid Soft Actuators. *Phys. Chem. Chem. Phys.* **2021**, *23*, 6710–6716, https://doi.org/10.1039/D1CP00289A.

46. Peniche, C.; Argüelles-Monal, W.; Davidenko, N.; Sastre, R.; Gallardo, A.; San Román, J. Self-Curing Membranes of Chitosan/PAA IPNs Obtained by Radical Polymerization: Preparation, Characterization and Interpolymer Complexation. *Biomaterials* **1999**, *20*, 1869–1878, https://doi.org/10.1016/S0142-9612(99)00048-4.

47. Yiamsawas, D.; Kangwansupamonkon, W.; Chailapakul, O.; Kiatkamjornwong, S. Synthesis and Swelling Properties of Poly[Acrylamide-Co-(Crotonic Acid)] Superabsorbents. *React. Funct. Polym.* **2007**, *67*, 865–882, https://doi.org/10.1016/J.REACTFUNCTPOLYM.2007.05.011.

48. Bajpai, A.K.; Shrivastava, M. Swelling Kinetics of a Hydrogel of Poly(Ethylene Glycol) and Poly(Acrylamide-Co-Styrene). *J. Appl. Polym. Sci.* **2002**, *85*, 1419–1428, https://doi.org/10.1002/APP.10675.

49. Ozcan, N.; Saloglu, D. Swelling Kinetics and Diffusion Coefficients of Polyacrylamide Hydrogels Via Different Drying Methods. *J. Chem. Eng. Res. Updat.* **2015**, *2*, 51–56, https://doi.org/10.15377/2409-983X.2015.02.02.2.